Title Page

Dihydromyricetin Inhibits Inflammation of Fibroblast-like Synoviocytes through Regulation of NF-κB Signaling in Collagen-Induced Arthritis Rats

Jing Wu[1#], Fu-Tao Zhao[2#], Kai-Jian Fan[1], Jun Zhang[3], Bing-Xing Xu[1], Qi-Shan Wang[1], Ting-Ting Tang[4], Ting-Yu Wang[1]*

1 Department of Pharmacy, Shanghai Ninth People's Hospital, Shanghai Jiao Tong University School of Medicine, Shanghai, People's Republic of China

2 Department of Rheumatology and Immunology, Shanghai Ninth People's Hospital, Shanghai Jiao Tong University School of Medicine, Shanghai, People's Republic of China

3 Department of Surgical Oncology, The University of Texas MD Anderson Cancer Center, Houston, TX 77030, USA

4 Shanghai Key Laboratory of Orthopaedic Implants, Department of Orthopaedic Surgery, Shanghai Ninth People's Hospital, Shanghai Jiao Tong University School of Medicine, Shanghai 200011, China

# Jing Wu and Fu-Tao Zhao contributed equally to this work.

* Corresponding author.

This work was supported by National Natural Science Foundation of China (NSFC) [grant # 81874011, 81572104 and 81301531] to TY Wang. This work was also partially supported by the Innovation Grant from Shanghai Municipal Science and Commission [grant #18140903502] to TY Wang.

Running Title Page

DMY Inhibits FLSs Inflammation in CIA Rats

Correspondence to: Dr. Ting-Yu Wang, Department of Pharmacy, Shanghai Ninth People's Hospital, Shanghai Jiao Tong University School of Medicine, Shanghai, China. Tel & Fax: +86 21 53315368, E-mail: drtywang@163.com

Number of text pages: 43

Number of tables: 0

Number of figures: 6

Number of references: 57

The number of words in the Abstract: 250

The number of words in the Introduction: 536

The number of words in the Discussion: 892

ABBREVIATIONS: BSA, albumin from bovine serum; CII, collage II; CCK-8, cell counting kit-8; CIA, collagen-induced arthritis; CO_2, carbon dioxide; Ct, threshold cycle; DAPI, 4', 6-diamidino-2-phenylindole; DMEM, dulbecco's modified eagle's medium; DMY, dihydromyricetin; ELISA, enzyme-linked immunosorbent assay; FBS, fetal bovine serum; FLSs,

fibroblast-like synoviocytes; GAPDH, glyceraldehyde-3-phosphate dehydrogenase; H & E, hematoxylin and eosin; HPLC, high purity liquid chromatography; i.d., intradermal injection; IκBα, inhibitor of NF-κB alpha; IF, immunofluorescence; IFA, incomplete freund 's adjuvant; IKK, IκB kinase; IL, interleukin; i.p., intraperitoneal; MMPs, matrix metalloproteinases; NF-κB, nuclear factor κ-light-chain-enhancer of activated B cells; OD, optical density; PBS, phosphate-buffered formalin; PFA, paraformaldehyde; PI, propidium iodide; PMSF, phenylmethanesulfonyl fluoride; RA, rheumatoid arthritis; RANKL, receptor activator of NF-κB ligand; RIPA, radioimmunoprecipitation assay lysis buffer; TNF-α, tumor necrosis factor α.

The recommended section assignment: Cellular and Molecular; Inflammation; Immunopharmacology.

Abstract

Dihydromyricetin (DMY), the main flavonoid of *Ampelopsis grossedentata*, has a potent anti-inflammation activity. However, the effect of DMY on the chronic autoimmune arthritis remains undefined. In this study we investigated the therapeutic effects of DMY on collagen-induced arthritis (CIA). Wistar rats were immunized with bovine type II collagen to establish CIA and then administered intraperitoneally (i.p.) with DMY (5, 25 and 50 mg/kg) every other day for five weeks. Paw swelling, clinical scoring and histologic analysis were performed to determine the therapeutic effects of DMY on arthritis development in CIA rats. The results showed that treatment with DMY significantly reduced the erythema and swelling in the paws of CIA rats. The pathological analysis of the knee joints and the peripheral blood cytokine assay confirmed the anti-arthritic effects of DMY on synovitis and inflammation. Fibroblast-like synoviocytes (FLSs) were isolated from the synovium of CIA rats and treated with 10 ng/ml interleukin (IL)-1β. DMY significantly inhibited the proliferation, migration and inflammation of IL-1β-induced FLSs, while it significantly increased IL-1β-induced FLSs apoptosis in a dose-dependent manner (6.25-25 μM). Moreover, DMY suppressed the phosphorylation of IκB kinase (IKK) and inhibitor of NF-κB alpha (IκBα), and subsequently reduced IL-1β-induced nucleus translocation of NF-κB in FLSs. Through molecular docking assay we demonstrated that DMY could directly bind to the Thr9 and Asp88 residues in IKKα and the Asp95, Asn142, and Gln167 residues in IKKβ. These findings demonstrated that DMY could alleviate inflammation in CIA rats and attenuate IL-1β-induced activities in FLSs through suppressing the NF-κB signaling.

Introduction

Rheumatoid arthritis (RA) is a chronic and systemic autoimmune polyarthritis characterized by the progressive exacerbation of multiple joints. There is a massive influx of immune cells into the synovial tissue during the progression of articular destruction that eventually leads to joint swelling, stiffness, deformity and dysfunction of affected joints in patients (Mcinnes and Schett, 2007; Boissier et al., 2012; Bt et al., 2013; Firestein, 2003). In normal synovium, fibroblast-like synoviocytes (FLSs) are responsible for governing the provision of support, nourishment, and lubrication of the joint tissue (Karouzakis et al., 2009). However, when the infiltration of several types of immune cells occurs in the synovial fluid, FLSs become hyperplastic and highly migratory, contributing to the progressive destruction of cartilage and bone. It has been reported that FLSs isolated from arthritic mice can invade healthy joints when transferred to nonarthritic mice (Müllerladner et al., 2005; Mor et al., 2005). Additionally, FLSs intends to release proinflammatory cytokines, proteases, growth factors and chemokines that recruit and activate peripheral mononuclear cells, neutrophils, macrophages, and mast cells to form an autocrine loop, resulting in extensive cartilage and bone deterioration (Cope, 2008; Drexler et al., 2008; Guma et al., 2010). Thus, FLSs could be a potential target for the treatment of RA. However, there is no specific FLSs-targeted or FLSs-inhibited drug for RA treatment.

Dihydromyricetin (DMY), a type of flavonoid, is the main bioactive component of *Ampelopsis grossedentata* which is a widely distributed herbal medicine in Southern China (Okazaki et al., 2005). Previous reports have demonstrated that DMY has numerous biological and pharmacological activities, including antioxidative, anti-inflammatory, antiapoptotic, anticarcinogenic and antidiabetic effects (Le et al., 2016; Li et al., 2015;Wu et al., 2016; Ye et al.,

2015; Chen et al., 2015). Considering that DMY possesses an anti-inflammatory property, we investigated its potential capacity to inhibit the chronic autoimmune inflammation of RA. Nuclear factor κ-light-chain-enhancer of activated B cells (NF-κB) plays a crucial role in the expression of various proinflammatory mediators (Mcinnes and Schett, 2007; Ivashkiv, 2011). An increasing number of studies have demonstrated that the NF-κB pathway is one of the key signaling pathways in promoting joint inflammation (Okazaki et al., 2005; Hah et al., 2010) and FLSs proliferation (Murphy and Nagase, 2008; Vincenti et al., 1998) in RA. Previous results demonstrated that NF-κB binding is significantly higher in RA synovium compared to that of osteoarthritis (Okazaki et al., 2005). Whether DMY inhibits RA through regulating NF-κB signaling pathway requires further investigation.

Collagen-induced arthritis (CIA) is an autoimmune disease animal model mainly characterized by chronic synovitis concomitant with progressive destruction of joints. The pathological and immunological features of CIA are consistent with those of RA (Brenner et al., 2007; Larsson et al., 2005; Nieto et al., 2015). Similar to human RA, CIA displays several clinical symptoms, such as the generation of proinflammatory cytokines, synovitis and erosion of bone (Cho et al., 2007). Thus, CIA is a well-established and the clinically relevant model of RA (Hegen et al., 2008). In the present study, we chose rat CIA animal model to investigate the anti-arthritic effects of DMY on the development and progression of CIA. We aim to further evaluate whether DMY exerts suppressive effect on the FLSs activity through regulation of NF-κB signaling pathway.

Materials and Methods

Animals

Male Wistar rats, aged 7-8 weeks, were used in experiments and housed in SPF facilities in pathogen-free conditions. They were fed ad libitum and distributed in cages randomly. All experiments were conducted in strict conformance with the guidelines adopted from the U.S. National Institutes of Health for the Care and Use of Laboratory Animals and approved by the Ethics Committee of Shanghai Ninth People's Hospital, Shanghai Jiao Tong University School of Medicine.

Induction of CIA and Drug Administration

Rats were immunized with an emulsion containing 100 μg bovine collage II (CII; Chondrex, Washington, USA) with 1-week interval. CII emulsified 1:1 in incomplete freund 's adjuvant (IFA; Chondrex, Washington, USA) was intradermal injected (i.d.) around the base of the tail on day -7 and the same emulsion was injected by the same route on day 0 (Brenner et al.,2007; Larsson et al., 2005). Three experimental groups were intraperitoneal injected (i.p.) with 5 mg/kg (5 mg DMY per kilogram rat body weight), 25 mg/kg and 50 mg/kg DMY, respectively and the same administrations were performed on the rats every other day for five weeks. Six rats in the normal group were injected with phosphate-buffered formalin (PBS) in the same way as those in the model group. Clinical monitoring of rats was performed twice a week after the second immunization to acquire body weight and test the volume of the hind paws. Simultaneously, rats were scored blindly on a scale from 0 to 3 per hind paw (0-12 per rat) (Leavenworth et al., 2013): 0, normal; 1, mild swelling and/or erythema confined to the midfoot or ankle joint; 2, moderate edematous swelling extending from the ankle to the metatarsal joints;

and 3, pronounced swelling encompassing the ankle, foot and digits. Immunized rats were divided randomly into 4 groups, vehicle control group, injected with PBS, and three DMY treated groups (n = 7 in each group). DMY was high purity liquid chromatography (HPLC) grade, the molecular structure of which is (2R,3R)-3,5,7-trihydroxy-2-(3,4,5-trihydroxyphenyl)-2,3-dihydrochromen-4-one, ≥ 98% pure (Sigma-Aldrich, St. Louis, MO) and was administered i.p. in a dosage of 5, 25, or 50 mg/kg in 1 ml volume every other day.

Enzyme-linked Immunosorbent Assay (ELISA) of Inflammatory Cytokines

Peripheral blood was collected in centrifuge tubes after the last administration of DMY and underwent centrifugation at 3500 rpm for 10 min at room temperature with a cooling centrifuge until coagulation. The clear plasma layer was obtained and stored at -80°C in a deep freezer before assaying. The levels of cytokines interleukin (IL)-1β, tumor necrosis factor α (TNF-α) and IL-17A in the plasma of the experimental rats were detected by an ELISA kit (Multisciences, Hangzhou, China) according to standard protocols. The optical density (OD) was measured using an automatic microplate reader (Tecan Infinite M200 PRO NanoQuant, Switzerland) at a wavelength of 450 nm. Each sample was tested in duplicate, and concentrations were determined by reference to standard curves, generated by using the OD values of standard solutions with 1:2 serial dilutions, for estimating cytokine content.

Histopathological Analysis of Joints

On day 34 after the second immunization, the rats were anesthetized and rapidly sacrificed by cervical dislocation. Whole knee joints of the hind legs were carefully separated and fixed in 4% paraformaldehyde (PFA) for 24 h. The joints were decalcified in 0.5 M EDTA,

dehydrated through an alcohol gradient, embedded in paraffin wax, sectioned at 4 μm thickness in a sagittal plane and subjected to routine hematoxylin and eosin (H & E). Sections were photographed by a digital camera attached to the light microscope. The micrographs were evaluated by two blinded observers. To determine the histopathology of the joint, inflammatory activity was observed in the samples with H & E staining and scored from 0-3 according to the following criteria: 1 indicates mild inflammatory infiltration with no synovial lining cell hyperplasia; 2 indicates moderate infiltration with some synovial lining cell hyperplasia; and 3 indicates severe infiltration with marked synovial lining cell hyperplasia (Buttgereit et al., 2009).

Synovial Cell Culture and Stimulation

Synovial tissue specimens were isolated from rats with CIA and rinsed with PBS 2-3 times. Then, the tissues were minced into small blocks (~ 1 mm^3 pieces), transferred to a small culture flask and tiled uniformly with a spacing of approximately 1 mm. For air-liquid interface culture, each flask contained a small amount of Dulbecco's modified Eagle's medium (DMEM, Thermo Fisher Scientific, Rockford, IL) with high glucose supplemented with 10% fetal bovine serum (FBS, Gibco Life Technologies, Carlsbad, CA) and 1% antibiotics (penicillin and streptomycin) (Thermo Fisher Scientific, Rockford, IL) at 37°C in a humidified thermostatic incubator (Thermo Fisher Scientific, Rockford, IL) under 5% carbon dioxide (CO_2) to ensure that pieces adhered to the flask (Liu et al., 2017). After 4-6 h, an appropriate amount of fresh culture medium was added to the flask to continue the culture, and medium was totally exchanged every 2 days with the same volume of fresh DMEM. Within 7 days, FLSs could migrate out from the tissue explant and achieve approximately 80% confluency (Shang et al., 2017), then, the tissues were removed, and the liberated FLSs were trypsinized, collected, re-

suspended, planted for expansion and used at passage 3 to 6 (Angiolilli et al., 2017; Xiao et al., 2014).

Identification of FLSs

FLSs migrated from synovial tissues on day 0, 4, 5, 6 were observed. FLSs were seeded into a 6-well plate with 8×10^4 cells/ well and cultured for 24 h. The cells were fixed with 100% methanol for 5min, permeabilized with 0.1% Triton X-100 for 5 minutes and then blocked with 1% BSA in 0.1% PBS-Tween for 1h. Immunofluorescence staining of FLSs with purified anti-Vimentin antibody (Abcam, Cambridge, UK) at a working dilution of 1/250 overnight at 4℃ and followed by a further incubation at room temperature for 1h with goat anti-rabbit IgG secondary antibody (dilution 1:300, Santa Cruz Biotechnology, Dallas, TX, USA). Nuclear DNA was labelled with 4', 6-diamidino-2-phenylindole (DAPI, Sigma-Aldrich, St. Louis, MO) (Fan et al., 2017; Yang et al., 2017). In addition, phenotype identification and purity analysis of FLSs was performed by fluorescence-activated cell sorting (FACS) analysis (Doss et al., 2016). FLSs were seeded into a 6-well plate with 3×10^5 cells per well and collected after cultivation for 24 h. Cells were then re-suspended with 100 μl FACS buffer (1 % BSA in 1× PBS) containing 0.5 mg/ml fluorescein isothiocyanate (FITC)-conjugated monoclonal CD90 (also called Thy-1 or Thy1) antibody (Biolegend, San Diego, CA, USA) and incubated at 4℃ for 30 min under dark conditions. Analysis was conducted by flow cytometer (BD LSRFortessa X-20 cell analyzer, San Diego, CA).

Cell Proliferation Assay

Cytotoxicity experiments were performed to measure cell proliferation after administering DMY to synovial cells alone. In general, FLSs were seeded in 96-well plates (Corning Glassworks, Corning, NY) with 2500 cells per well; 24 h later, they were randomized into four groups and treated with vehicle or a test compound DMY (3.125-800 μM) for 24 and 48 h. All tests were performed in triplicate, and cell proliferation rates were assessed by the Cell Counting Kit-8 (CCK-8; Dojindo, Japan) following the manufacturer's recommendation. At each time point, the absorbance was measured at 450 nm using a microplate reader (Shang et al., 2017). To detect the inhibitory effect of DMY on FLSs, cells were stimulated with 10 ng/mL IL-1β (R & D Systems, Minneapolis, MN) to maintain the condition of inflammation and then incubated in the presence of DMY at different concentrations.

In Vitro Migration Assay

The migration ability of the FLSs was evaluated in a 24-well micro chemotaxis chamber (Corning BioCoat, Shanghai, China) with an 8 μm pore size. DMY and cells in DMEM without FBS were loaded into the upper chambers, and 10% FBS media was added into the lower chambers to evaluate the effect of DMY on migration. After 16 h, a cotton swab was used to remove the remaining cells from the upper surface of the filter, and the cells adhering beneath were fixed in 4% PFA for 20 min and dyed with 0.1% crystal violet for 30 min. Migrated cells were counted in five random fields for each assay at 20× magnification using light microscopy (Shang et al., 2017). In addition, a scratch wound assay in vitro was adopted to evaluate FLSs migration. FLSs were seeded in 60 mm culture dishes (Corning Glassworks, Corning, NY) at a density of 5×10^5 cells/ml; when they reached 90% confluence, one parallel wound was created using a sterile 200 μl pipette tip. The detached cells were washed away by serum-free media, and

then the cultured FLSs were treated with DMY (various concentrations such as 6.25, 12.5, 25 μM) without FBS. Photographs were taken at the indicated time points (0, 16, 24, 48 h), and migration was quantified by calculating the percentage of the area of FLSs migrating to the scratch with Image J software (Wang et al., 2016).

Flow Cytometric Analysis of Apoptosis

For apoptosis analysis, FLSs were exposed to several concentrations (6.25, 12.5, 25 μM) of DMY in DMEM for 24 h. Approximately 5×10^5 cells were collected and stained with an Annexin V (AV)-APC/propidium iodide (PI) apoptosis kit (eBioscience, San Diego, CA) following the manufacturer's protocol to be analyzed by flow cytometer (BD LSRFortessa X-20 cell analyzer, San Diego, CA). Early apoptotic cells were defined as Annexin V-positive and PI-negative, in the lower-right quadrant of the graph, whereas late apoptotic cells were positive for both Annexin V and PI, in the upper-right quadrant. The percentages in these two quadrants were calculated to represent the total apoptotic rate (Liu et al., 2017; Shang et al., 2017).

Real-time Polymerase Chain Reaction (PCR)

After the same treatment as above, FLSs were homogenized in TRIzol reagent (Ambion, Shanghai, China) to extract total cellular RNA, which was subsequently reverse-transcribed to cDNA using the cDNA reverse transcription kit (Takara Bio, Tokyo, Japan) following the standard protocol. The real-time PCR primers for TNF-α, IL-1β, IL-6 and β-actin were synthesized by Shanghai SangonBiological Engineering Technology & Services

Co., Ltd. Primers were TNF-α (forward: 5′ ATGGGCTCCCTCTCATCAGT 3′; reverse: 5′ GCTTGGTGGTTTGCTACGAC 3′), IL-1β (forward: 5′ AGCAGCTTTCGACAGTGAGG 3′; reverse: 5′ CTCCACGGGCAAGACATAGG 3′), IL-6 (forward: 5′CTCTCCGCAAGAGACTT CCAG 3′; reverse: 5′ TTCTGACAGTGCATCATCGCT 3′), and β-actin (forward: 5′ ACGGTC AGGTCATCACTATCG 3′; reverse: 5′ GGCATAGAGGTCTTTACGGATG 3′). Quantitative real-time PCR was performed on a 7500 Real-Time PCR System (Thermo Fisher Scientific, Rockford, IL) according to the manufacturer's instructions. The cycling program was conducted as follows: predenaturation at 95°C for 30 min, then 40 cycles of denaturation at 95°C for 5 sec and annealing and extension at 60°C for 34 sec. Target gene expression was determined as fold induction relative to the housekeeping gene expressed as $2^{-\Delta Ct}$ value, where Δthreshold cycle (Ct) was calculated with the comparative Ct between β-actin, as the endogenous control, and the target gene (Anderson et al., 2015; Yeo et al., 2016).

Western Blotting

For each experiment, 3×10^5 cells/well were seeded in 6-well plates (Corning Glassworks, Corning, NY), when subconfluence (~70%) was reached, the FLSs were stimulated with 10 ng/ml IL-1β a serial of time points (15, 30, 45, 60 min) to determine an appropriate time point, and then pretreated with serial concentrations of DMY for 24 h and exposed to 10 ng/ml IL-1β for the desired time. Total cellular proteins were extracted by adding ice-cold radio immunoprecipitation assay lysis buffer (RIPA) (Beyotime, Shanghai, China) along with the protease inhibitor phenylmethanesulfonyl fluoride (PMSF) (100 mM, Biosharp, Wuhan, China) along with a phosphatase inhibitor cocktail (100×, Thermo Fisher Scientific, Rockford, IL). The FLSs were placed without shaking for 30 min; then, the cells were scraped off the plate, and the

whole-cell lysates were centrifuged at 14000 rcf for 15 min at 4°C (Xin et al., 2014). The obtained supernatants were mixed with 5 × protein loading dye (Sangon Biotech, Shanghai, China) with a ratio of 5:1 and boiled for 5 min. The blots were probed with primary Abs (dilution 1:1000; Cell Signaling Technology, Beverly, MA) against NF-κB p65, phospho-NF-κB p65, inhibitor of NF-κB alpha (IκBα), phospho-IκBα, phospho-IKKα/β, IκB kinase (IKK)α, IKKβ and glyceraldehyde-3-phosphate dehydrogenase (GAPDH) at 4°C overnight, followed by washing with Tris-buffered saline Tween 20 (TBST, Epizyme Scientific, Shanghai, China) and incubated with the corresponding secondary antibodys (dilution 1:10000; Cell Signaling Technology, Beverly, MA) for 1 h at room temperature (Li et al., 2017; Zhou et al., 2014). The expression of each signal protein was shown as the ratio of the staining intensity for the target protein to that for GAPDH (Qiao et al., 2016). The band intensity was quantified by Image J software.

Immunofluorescence (IF) Staining

FLSs cultured on confocal dishes were treated in the same way as for western blotting. Then, they were washed and fixed with 4% PFA for 30 min, permeabilized with 1% Triton X-100 for 30 min, blocked with 3% albumin from bovine serum (BSA) for 30 min at room temperature, and incubated with primary anti-NF-κB-p65 antibody (dilution 1:400; Cell Signaling Technology, Beverly, MA) overnight at 4°C and CY3-labeled goat anti-rabbit IgG as secondary antibody (dilution 1:300, Santa Cruz Biotechnology, Dallas, TX, USA) at room temperature for 1 h. The nuclei were visualized using DAPI (Xin et al., 2014; Li et al., 2017).

Molecular Modeling

DMY and the rat IKK proteins were preprocessed by Ligprep 3.4 software (Schrödinger, USA) and Protein Preparation Wizard software (Schrödinger, USA), respectively. In silico docking was subsequently performed using the standard precision scoring function of Glide 5.5 software (Schrödinger, USA) with default values for other parameters.

Results

DMY Inhibits CIA Development in Rats

To investigate the therapeutic effects of DMY on autoimmune arthritis, DMY was administered (i.p.) to CIA rats every other day for five weeks. Evident swelling, erythema, edema and joint rigidity confined to the paws of the rats in the vehicle-treated group appeared on day 10 and increasing aggravation of paw swelling was observed in the following week especially reached a plateau on day 18 after strengthened immunizationon (Figure 1A). The intensity of arthritis was evaluated in term of hind paw swelling, loss of weight and clinical score since the day of the second immunization. The weights of the CIA rats in the placebo group were lighter than normal, whereas the rats in the experimental groups treated with different doses of DMY had increased body weight first and then gradually returned to the normal body weight. Additionally, the degrees of swelling and arthritic scores were alleviated dramatically, especially at the high dose of DMY (Figure 1B). Therefore, the change in clinical symptoms of CIA rats suggest that DMY could inhibit arthritis significantly.

DMY Attenuates Systemic Inflammation in CIA Rats

At the end of follow-up (d34), the levels of proinflammatory cytokines (IL-1β, TNF-α and IL-17A) in the plasma of the peripheral blood were detected by ELISA. Compared to those in the vehicle-treated group, the levels of detected inflammatory cytokines were reduced in a dose-dependent manner in the groups treated with different doses of DMY (Figure 2A).

DMY Ameliorates Joint Injury and Inflammatory Infiltration in CIA Rats

The inflamed joints in the vehicle treated CIA group showed clear rheumatoid inflammation presenting as synovial hyperplasia with intense inflammatory cell infiltration compared to the joints of normal rats. DMY could ease the deleterious effects of inflammatory arthritis in CIA rats, demonstrated by the histologic analysis (Figure 2B). Histologic scores for synovitis showed that DMY markedly arrested articular destruction of CIA rats in a dose-dependent manner (Figure 2C).

DMY Inhibits Cellular Activities in IL-1β Stimulated FLSs

We isolated FLSs from synovial tissues of CIA rats. The cells migrated out from the tissue explants were shuttle-shaped or polygonal that conform to morphological characteristics of fibroblasts (Figure 3A). Vimentin is positively expressed in 100% of FLSs (Figure 3B). CD90 was the molecule that specifically expressed in FLSs and our results showed 95.56% of FLSs stained positive for CD90 (Figure 3C).

To rule out the possible toxic effects of DMY on FLSs, cells were exposed to increasing concentrations of DMY to detect cell viability in a CCK-8 assay. The results revealed that no notable cytotoxicity to RA-FLSs was observed 24 and 48 hours after DMY treatment (3.125-400 μM) (Figure 4A).

The inhibition of DMY on FLSs proliferation, apoptosis, migration and inflammation were detected in IL-1β (10 ng/ml) induced FLSs *in vitro*. We found that IL-1β promoted FLSs proliferation, whereas DMY abrogated the proliferation dose-dependently (Figure 4B). Annexin V/PI double staining was performed to detect the proapoptotic effects of different concentrations of DMY on IL-1β stimulated FLSs (Figure 4C). The results of counting the rates of Annexin V/PI double-positive cells revealed that IL-1β strikingly inhibited FLSs apoptosis; in contrast,

the level of cell apoptosis significantly increased with increasing concentrations of DMY (Figure 4D). We next investigated whether DMY suppresses the migratory capacity of FLSs with a Transwell and a wound closure assays. Firstly, we determined the appropriate period of migration was 16 hours (Figure 5A and B). Treatment with IL-1β significantly enhanced cell motility, causing a 2-3-fold increase in migrated cell numbers compared to that in the placebo group in transwell assay. In contrast, the treatment with DMY counteracted this trend and evidently abrogated the IL-1β-mediated FLSs migration (Figure 5C and D). Consistent with the above results, the erosion trace assay showed the same tendency (Figure 5E) and DMY possessed suppressive activity in a concentration-dependent manner in the wound-scratching assay (Figure 5F). Since inflammation is obvious in RA FLSs, it is reasonable to determine the effect of DMY on the expression of proinflammatory cytokines in FLSs. We evaluated the mRNA levels of several major inflammatory cytokines such as IL-6, TNF-α and IL-1β after exposure to different concentrations of DMY for 24 hours. In comparison to those in the control, reduced mRNA levels of these cytokines were observed in FLSs treated with different concentrations of DMY (Figure 6A). Collectively, consistent with the previous capacity of DMY on arthritis *in vivo*, DMY could substantially restrain the activity of IL-1β stimulated FLSs, providing a potential therapeutic effect of DMY on synovial hyperplasia and synovitis of arthritis.

DMY Inhibits FLSs through Regulation of NF-κB Signaling

Compared to that in control medium, the phosphorylation of NF-κB was apparently increased in IL-1β-induced FLSs. In addition, a time course analysis revealed that, under IL-1β stimulation for 15 min, activated IKK could promote the phosphorylation and proteolytic degradation of IκBα and the phosphorylation of NF-κB, contributing to the translocation of NF-

κB to the nucleus (Figure 6B). We further examined the effect of DMY on the NF-κB pathway in cultured FLSs. As shown in Figure 6C, pretreatment with DMY markedly inhibited the IL-1β-mediated phosphorylation of IKK, p65 and IκBα in a concentration-dependent manner. These results were further confirmed by IF staining using an anti-p65 antibody targeting to the major subunit of NF-κB to evaluate the effect of DMY on NF-kB activation and translocation. We found that DMY significantly reduced p65 nuclear translocation in IL-1β-induced FLSs (Figure 6D). The molecular docking assay demonstrated that DMY directly bound to the Thr9 and Asp88 residues in IKKα and the Asp95, Asn142, and Gln167 residues in IKKβ (Figure 6E). Collectively, our findings suggest that DMY suppressed IL-1β-induced phosphorylation of IKK, degradation of IκBα and nuclear translocation of NF-κB in FLSs through directly binding to the specific amino acid residues of IKK.

Discussion

The etiopathogenesis of RA is considered as multiple joints damage caused by abnormal immune regulation, in which synovitis is the typical pathological feature. Inflammation, loss of synovial homeostasis and progressive synovium-mediated joint destruction are typical features of inflammatory arthritis (Karouzakis et al., 2009). The synovium in RA manifests hyperplastic and invasive properties mediated by local lymphocytes in synovial tissue (Takemura et al., 2001). In addition, the balance between proteases and their inhibitors in normal synovium is broken by the excessive expression of matrix metalloproteinases (MMPs) that eventually leads to the destruction of cartilage and bone erosion (Garcia-Vicuna et al., 2004). In our study, we found that the paw volume and the arthritis score of CIA rats were progressively decreased, and the body weight was gradually increased with DMY administration (Figure 1). The systemic inflammation mediated by cytokines (including TNF-α, IL-1β and IL-l7A) in peripheral blood was substantially suppressed by the treatment of DMY. Moreover, the results of histologic analysis of knee joints in the animals administered with different doses of DMY showed decreased inflammatory cell infiltration and alleviated synovial hyperplasia. Taken together our results demonstrated that DMY could evidently abrogate synovitis and systemic inflammation in CIA rat.

Synovial cells contain type A or macrophage-like synovial cells and type B or FLSs of which type A cells possess little capacity to proliferate (Bartok and Firestein, 2010). FLSs hyperplasia in RA displays surprisingly pathogenic behavior to promote pannus growth, inflammation and destruction of the joint (Bottini and Firestein, 2013) so as to serves as the link between immune response and joint damage (Qu et al., 1994a). Thus, we focus on the inhibitory effects of DMY on arthritis by specifically targeting FLSs which provides nourishment, support,

and lubrication to the joint in the normal synovium and become highly hyperplastic and invasive in the inflammatory milieu. Since IL-1β levels in plasma of peripheral blood were significantly increased in CIA rats and IL-1β plays a key role in synovitis and joint destruction in patients with RA (Tak and Bresnihan, 2000), we choose IL-1β as the stimulatory cytokine in the *in vitro* experiments to maintain inflammatory state and invasive activity of FLSs similar to the *in vivo* arthritis status. Previous results demonstrated that synovitis is mainly mediated by FLSs, which possess the abilities of secreting proinflammatory cytokines as well as mediators of bone destruction such as MMPs and RANKL, attracting and activating proinflammatory cells in the inflamed joint (Bottini and Firestein, 2013; Goldring et al., 2013) and ultimately resulting in the destruction of the affected joints (Choy and Panayi, 2001; Rico et al., 2007). We evaluated the mRNA levels of several major inflammatory cytokines such as IL-6, TNF-α and IL-1β after exposure to different concentrations of DMY in IL-1β stimulated FLSs. In comparison to those in the control, reduced mRNA levels of these cytokines were observed in DMY groups dose-dependently (Figure 6A). The migratory capacity of FLSs was detected with Transwell and wound healing assays. DMY evidently abrogated the IL-1β-mediated FLSs migration in a concentration-dependent manner (Figure 5). Synovial hyperplasia is caused by restrained apoptosis concomitant with promoted proliferation of FLSs (Liu and Pope, 2003). The results showed that changes in FLSs proliferation and apoptosis observed in patients with RA may be caused by inactivation of p53, which leads to defects in antiproliferative and proapoptotic effects, similar to that in tumor cells (Lefèvre et al., 2009; Pap et al., 2004). We found that DMY exerts potent suppressive effect on IL-1β-mediated FLSs proliferation, while significant increased function on IL-1β-mediated FLSs apoptosis. Moreover, cell cytotoxicity assay showed no differences in cell viability between the different doses of DMY groups (6.25-25 μM) and the

vehicle control group. Thus, DMY may attenuate the arthritis of CIA rats by regulating the activities of inflammation, migration, proliferation and apoptosis of inflammatory FLSs.

The NF-κB pathway has been demonstrated to be highly activated in the conventional inflammation diseases (Miagkov et al., 1998; Tad and Bresnihan, 2000). NF-κB normally presents as a complex with IκBα in cytoplasm and can be released after the phosphorylation of IκBα which is mediated by the independent of IKKβ from IKKα in response to a cellular stimulation like proinflammatory cytokines (Bartok and Firestein, 2010). The IKK complex of IKKα and IKKβ is a convergence point for NF-κB signaling (Bartok and Firestein, 2010). The liberated NF-κB migrates into the nucleus to regulate the transcriptional activity of the target genes and precedes the deterioration of synovial inflammation in RA (Tad and Bresnihan, 2000). Previous studies have also revealed that DMY can decrease the quantity of receptor activator of NF-κB ligand (RANKL) to suppress the activation of NF-κB and the phosphorylation of p38, resulting in lowering serum levels of inflammatory cytokines in pharyngitis and decreasing bone loss in osteoporosis (Zhao et al., 2017; Hou et al., 2015). We demonstrated that DMY significantly attenuates the IL-1β-induced phosphorylation of IKK and IκBα, thereby decreasing NF-κB translocation into the nucleus and consequently regulating the transactivation of NF-κB dependent genes such as proinflammatory cytokines. Molecular docking of IKKα and IKKβ with DMY further demonstrated that DMY could down-regulate NF-κB signaling by direct binding to IKK thus inhibiting IKK phosphorylation.

Overall, this study clearly demonstrated that DMY exerts the anti-arthritic effect in CIA rats through regulation of the NF-κB signaling of FLSs. Our findings suggest that DMY may ~~be~~ serve as a potential key therapeutic agent for RA treatment.

Authorship Contributions

Participated in research design: TY Wang, J Wu.

Conducted experiments: J Wu, FT Zhao, KJ Fan, BX Xu, QS Wang

Contributed new reagents or analytic tools: J Wu, J Zhang, TT Tang, TY Wang

Performed data analysis: J Wu, TY Wang

Wrote or contributed to the writing of the manuscript: J Wu, FT Zhao, TY Wang

References

Anderson AE, Pratt AG, Sedhom MA, Doran JP, Routledge C, and Hargreaves B, et al (2015) IL-6-driven STAT signalling in circulating $CD4^+$ lymphocytes is a marker for early anticitrullinated peptide antibody-negative rheumatoid arthritis. *Ann Rheum Dis* 75: 466-473.

Angiolilli C, Kabala PA, Grabiec AM, Baarsen IMV, Ferguson BS, and García S, et al (2017) Histone deacetylase 3 regulates the inflammatory gene expression programme of rheumatoid arthritis fibroblast-like synoviocytes. *Ann Rheum Dis* 76: 277-285.

Bartok B and Firestein GS (2010) Fibroblast-like synoviocytes: key effector cells in rheumatoid arthritis. *Immunol Rev* 233: 233-255.

Boissier MC, Semerano L, Challal S, Saidenberg-Kermanac'H N, and Falgarone G (2012) Rheumatoid arthritis: from autoimmunity to synovitis and joint destruction. *J Autoimmun* 39: 222-228.

Bottini N, and Firestein GS (2013) Duality of fibroblast-like synoviocytes in RA: passive responders and imprinted aggressors. *Nat Rev Rheumatol* 9: 24-33.

Brenner, M., Laragione, T., Mello, A., and Gulko, P. S (2007) Cia25 on rat chromosome 12 regulates severity of autoimmune arthritis induced with pristane and with collagen. *Ann Rheum Dis* 66: 952-957.

Bt VDB, Abdollahiroodsaz S, Vermeij EA, Bennink MB, Arntz OJ, and Rothlin CV, et al (2013) Therapeutic efficacy of Tyro3, Axl, and Mer tyrosine kinase agonists in collagen-induced arthritis. *Arthritis Rheum* 65: 671-680.

Buttgereit F, Zhou H, Kalak R, Gaber T, Spies CM, and Huscher D, et al (2009) Transgenic disruption of glucocorticoid signaling in mature osteoblasts and osteocytes attenuates K/BxN mouse serum–induced arthritis in vivo. *Arthritis Rheum* 60: 1998-2007.

Chen S, Zhao X, Jing W, Li R, Yu Q, and Wang X, et al (2015) Dihydromyricetin improves glucose and lipid metabolism and exerts anti-inflammatory effects in nonalcoholic fatty liver disease: A randomized controlled trial. *Pharmacol Res* 99: 74-81.

Cho YG, Cho ML, Min SY, and Kim HY (2007) Type Ⅱ collagen autoimmunity in a mouse model of human rheumatoid arthritis. *Autoimmun Rev* 7: 65-70.

Choy EH, and Panayi GS (2001) Cytokine pathways and joint inflammation in rheumatoid arthritis. *N Engl J Med* 344: 907-916.

Cope AP (2008) T cells in rheumatoid arthritis. *Arthritis Res Ther* 10 (Suppl 1): S1.

Doss, H. M., Ganesan, R., and Rasool, M (2016) Trikatu, an herbal compound ameliorates rheumatoid arthritis by the suppression of inflammatory immune responses in rats with adjuvant-

induced arthritis and on cultured fibroblast like synoviocytes via the inhibition of the nfκb signaling pathway. *Chem Biol Interact* 258: 175-186.

Drexler SK, Kong PL, Wales J, and Foxwell BM (2008) Cell signalling in macrophages, the principal innate immune effector cells of rheumatoid arthritis. *Arthritis Res Ther* 10: 216.

Fan, P., He, L., Hu, N., Luo, J., Zhang, J., and Mo, L. F., et al (2017) Effect of 1,25-(OH)2D3 on proliferation of fibroblast-like synoviocytes and expressions of pro-inflammatory cytokines through regulating microRNA-22 in a rat model of rheumatoid arthritis. *Cell Physiol* 42: 145-155.

Firestein GS (2003) Evolving concepts of rheumatoid arthritis. *Nature* 423: 356-361.

García-Vicuña R, Gómez-Gaviro MV, Domínguez-Luis MJ, Pec MK, González-Alvaro I, Alvaro-Gracia JM, and Díaz-González F (2004) CC and CXC chemokine receptors mediate migration, proliferation, and matrix metalloproteinase production by fibroblastlike synoviocytes from rheumatoid arthritis patients. *Arthritis Rheum* 50: 3866-3877.

Goldring SR, Purdue PE, Crotti TN, Shen Z, Flannery MR, and Binder NB, et al (2013) Bone remodelling in inflammatory arthritis. *Ann Rheum Dis* 72: 52-55.

Guma M, Kashiwakura J, Crain B, Kawakami Y, Beutler B, Firestein GS, Kawakami T, Karin M, and Corr M (2010) JNK1 controls mast cell degranulation and IL-1beta production in inflammatory arthritis. *Proc Natl Acad Sci USA* 107: 22122-22127.

Hah YS, Lee YR, Jun JS, Lim HS, Kim HO, and Jeong YG, et al (2010) A20 suppresses inflammatory responses and bone destruction in human fibroblast-like synoviocytes and in mice with collagen-induced arthritis. *Arthritis Rheum* 62: 2313-2321.

Hegen M, Jr KJ, Collins M, and Nickerson-Nutter CL (2008) Utility of animal models for identification of potential therapeutics for rheumatoid arthritis. *Ann Rheum Dis* 67: 1505-1515.

Hou XL, Tong Q, Wang WQ, Shi CY, Xiong W, and Chen J, et al (2015) Suppression of inflammatory responses by dihydromyricetin, a flavonoid from ampelopsis grossedentata, via inhibiting the activation of NF-κB and MAPK signaling pathways. *J Nat Prod* 78: 1689-1696.

Ivashkiv LB (2011) Inflammatory signaling in macrophages: transitions from acute to tolerant and alternative activation states. *Eur J Immunol* 41: 2477-2481.

Karouzakis E, Gay RE, Gay S, and Neidhart M (2009) Epigenetic control in rheumatoid arthritis synovial fibroblasts. *Nat Rev Rheumatol* 5: 266-272.

Larsson, E., Harris, H. E., Palmblad, K., Månsson, B., Saxne, T., and Klareskog, L (2005) Cni-1493, an inhibitor of proinflammatory cytokines, retards cartilage destruction in rats with collagen induced arthritis. *Ann Rheum Dis* 64: 494–496.

Le L, Jiang B, Wan W, Zhai W, Xu L, and Hu K, et al (2016) Metabolomics reveals the protective of dihydromyricetin on glucose homeostasis by enhancing insulin sensitivity. *Sci Rep* 6: 36184.

Leavenworth JW, Tang X, Kim HJ, Wang X, and Cantor H (2013) Amelioration of arthritis through mobilization of peptide-specific CD8+ regulatory T cells. *J Clin Invest* 123: 1382-1389.

Lefèvre S, Knedla A, Tennie C, Kampmann A, Wunrau C, and Dinser R, et al (2009) Synovial fibroblasts spread rheumatoid arthritis to unaffected joints. *Nat Med* 15: 1414-1420.

Li N, Xu Q, Liu Q, Pan D, Jiang Y, and Liu M, et al (2017) Leonurine attenuates fibroblast-like synoviocyte-mediated synovial inflammation and joint destruction in rheumatoid arthritis. *Rheumatology* 56: 1417-1427.

Li T, Wong VKW, Zhi HJ, Shui PJ, Yan L, and Wang TY, et al (2015) Mutation of cysteine 46 in IKK-beta increases inflammatory responses. *Oncotarget* 6: 31805-31819.

Liu H, and Pope RM (2003) The role of apoptosis in rheumatoid arthritis. *Curr Opin Pharmacol* 3: 317-322.

Liu Y, Pan YF, Xue Y Q, Fang LK, Guo XH, and Guo X, et al (2017) Upar promotes tumor-like biologic behaviors of fibroblast-like synoviocytes through pi3k/akt signaling pathway in patients with rheumatoid arthritis. *Cell Mol Immunol* 15: 171-181.

Mcinnes IB, and Schett G (2007) Cytokines in the pathogenesis of rheumatoid arthritis. *Nat Rev Immunol* 7: 429-442.

Miagkov AV, Kovalenko DV, Brown CE, Didsbury JR, Cogswell JP, Stimpson SA, Baldwin AS, and Makarov SS (1998) NF-kappaB activation provides the potential link between inflammation and hyperplasia in the arthritic joint. *Proc Natl Acad Sci USA* 95: 13859-13864.

Mor A, Abramson SB, and Pillinger MH (2005) The fibroblast-like synovial cell in rheumatoid arthritis: a key player in inflammation and joint destruction. *Clin Immunol* 115: 118-128.

Müllerladner U, Pap T, Gay RE, Neidhart M, and Gay S (2005) Mechanisms of disease: the molecular and cellular basis of joint destruction in rheumatoid arthritis. *Nat Clin Pract Rheumatol* 1: 102-110.

Murphy G, and Nagase H (2008) Progress in matrix metalloproteinase research. *Molecular Mol Aspects Med* 29: 290-308.

Nieto, F. R., Clark, A. K., John, G., Victoria, C., and Marzia, M (2015). Calcitonin gene-related peptide-expressing sensory neurons and spinal microglial reactivity contribute to pain states in collagen-induced arthritis:. *Arthritis Rheum* 67: 1668-1677.

Okazaki Y, Sawada T, Nagatani K, Komagata Y, Inoue T, and Muto S, et al (2005) Effect of nuclear factor-kappaB inhibition on rheumatoid fibroblast-like synoviocytes and collagen induced arthritis. *J Rheumatol* 32: 1440-1447.

Pap T, Nawrath M, Heinrich J, Bosse M, Baier A, and Hummel KM, et al (2004) Cooperation of Ras- and c-Myc-dependent pathways in regulating the growth and invasiveness of synovial fibroblasts in rheumatoid arthritis. *Arthritis Rheum* 50: 2794-2802.

Qiao H, Wang T, Yu Z, Han X, Liu X, and Wang Y, et al (2016) Structural simulation of adenosine phosphate via plumbagin and zoledronic acid competitively targets JNK/Erk to synergistically attenuate osteoclastogenesis in a breast cancer model. *Cell Death Dis* 7: e2094.

Qu Z, Garcia CH, O'Rourke LM, Planck SR, Kohli M, and Rosenbaum JT (1994a) Local proliferation of fibroblast-like synoviocytes contributes to synovial hyperplasia. Results of proliferating cell nuclear antigen/cyclin, c-myc, and nucleolar organizer region staining. *Arthritis Rheum* 37: 212-220.

Rico MC, Castaneda JL, Manns JM, Uknis AB, Sainz IM, and Safadi FF, et al (2007) Amelioration of inflammation, angiogenesis and CTGF expression in an arthritis model by a TSP1-derived peptide treatment. *J Cell Physiol* 211: 504–512.

Shang-ling, Jian-lin, Huang, Wei-xiang, Peng, and Dan-chun, et al (2017) Inhibition of smoothened decreases proliferation of synoviocytes in rheumatoid arthritis. *Cell Mol Immunol* 14: 214-222.

Tad PP and Bresnihan B (2000) The pathogenesis and prevention of joint damage in rheumatoid arthritis: advances from synovial biopsy and tissue analysis. *Arthritis Rheum* 43: 2619-2633.

Tak PP and Bresnihan B (2000) The pathogenesis and prevention of joint damage in rheumatoid arthritis: advances from synovial biopsy and tissue analysis. *Arthritis Rheum* 43: 2619 – 2633.

Takemura S, et al. (2001) Lymphoid neogenesis in rheumatoid synovitis. *J Immunol* 167: 1072-1080.

Vincenti MP, Coon CI, and Brinckerhoff CE (1998) Nuclear factor kappaB/p50 activates an element in the distal matrix metalloproteinase 1 promoter in interleukin-1beta-stimulated synovial fibroblasts. *Arthritis Rheum* 41: 1987-1994.

Wang W, Miao Q, Lan X, Wu X, Zhen G, and Gu T, et al (2016) Sorafenib exerts an anti-keloid activity by antagonizing TGF-β/Smad and MAPK/ERK signaling pathways. *J Mol Med* 94: 1181-1194.

Wu Y, Bai J, Zhong K, Huang Y. and Gao H (2016) A dual antibacterial mechanism involved in membrane disruption and DNA binding of 2R,3R-dihydromyricetin from pine needles of Cedrus deodara against Staphylococcus aureus. *Food Chem* 218: 463-470.

Xiao Y, Sun M, Zhan Z, Ye Y, Huang M, and Zou Y, et al (2014) Increased phosphorylation of ezrin is associated with the migration and invasion of fibroblast-like synoviocytes from patients with rheumatoid arthritis. *Rheumatology* 53: 1291-1300.

Xin W, Huang C, Zhang X, Xin S, Zhou Y, and Ma X, et al (2014) Methyl salicylate lactoside inhibits inflammatory response of fibroblast‐like synoviocytes and joint destruction in collagen‐induced arthritis in mice. *Br J Pharmacol* 171: 3526-38.

Yang, Y., Dong, Q., and Li, R (2017) Matrine induces the apoptosis of fibroblast-like synoviocytes derived from rats with collagen-induced arthritis by suppressing the activation of the JAK/STAT signaling pathway. *Int J Mol Med* 39: 307-316.

Ye L, Wang H, Duncan SE, Eigel WN, and O'Keefe SF (2015) Antioxidant activities of Vine Tea (Ampelopsis grossedentata) extract and its major component dihydromyricetin in soybean oil and cooked ground beef. *Food Chem* 172: 416-422.

Yeo L, Adlard N, Biehl M, Juarez M, Smallie T, and Snow M, et al (2016) Expression of chemokines CXCL4 and CXCL7 by synovial macrophages defines an early stage of rheumatoid arthritis. *Ann Rheum Dis* 75: 763-771.

Zhao L, Cai C, Wang J, Zhao L, Li W, and Liu C, et al (2017) Dihydromyricetin protects against bone loss in ovariectomized mice by suppressing osteoclast activity. *Front Pharmacol* 8: 928.

Zhou, H. F., Yan, H., Pan, H., Hou, K. K., Akk, A.,and Springer, L. E., et al (2014) Peptide-siRNA nanocomplexes targeting NF-κB subunit p65 suppress nascent experimental arthritis. *Clin Invest* 124: 4363-4374.

Legends for Figures

Figure 1. DMY inhibits arthritis development in CIA rats. (A) A graphic scheme of CIA induction and DMY administration. Wistar rats were injected with the emulsion or PBS with one-week interval as described in methods. After second injection, rats (n = 6-7 per group) receiving DMY for five weeks and evaluation was conducted twice a week. (B) Hind paws swelling of rats were measured by two independent blinded observers from the second injection onward. On day 18, the volume of the paw in the CIA model reached to the peak and from day 14, the value of the DMY treated group was significantly lower than the vehicle group. Weight of rats in the group injected with DMY versus the vehicle differed significantly especially in two groups of higher doses. The values are presented as the mean ± S.E.M. (6-7 rats per group). $^{\#\#}P < 0.01$, $^{\#}P < 0.05$ versus the normal group; $^{**}P < 0.01$, $^{*}P < 0.05$ versus the vehicle-treated group.

Figure 2. DMY Suppresses inflammation in CIA Rats. (A) Plasma cytokine levels. Cytokine levels were quantified in supernatants of peripheral blood isolated on day 34 of CIA rats by ELISA. The plasma of rats administered with DMY *in vivo* contain significantly less IL-1β, TNF-α and IL-17A than untreated CIA rats. (B) Representative joint sections stained with hematoxylin and eosin (H & E). The black boxes represent the areas of the magnification of the figure which showed on the below. The synovial tissue of the knee joint of CIA rats displayed evident synovial hyperproliferation (SH) and inflammatory cell infiltration (ICI). While, in the DMY-treated CIA and normal group, knee joints had slight inflammatory cell infiltration. Scale bar = 200 μm (upper panel) and 100 μm (lower panel). (C) Histologic scores for inflammation in rats treated with DMY or vehicle are shown. Results are presented as the mean ± S.E.M. (n = 6-7

rats per group). $^{\#\#}P < 0.01$, $^{\#}P < 0.05$ versus the normal group; $^{**}P < 0.01$, $^{*}P < 0.05$ versus the vehicle-treated group.

Figure 3. Phenotype and purity analysis of FLSs. (A) Representative images of FLSs migrated from synovial tissues on day 0, 4, 5 and 6. (B) IF images of FLSs stained with vimentin (green) have been showed. As presented in images, vimentin, found in connective tissue and cytoskeleton, nearly expressed in all FLSs. Bar = 10 μm. (C) Fluorescence-activated cell sorting (FACS) analysis of FLSs stained with fluorescein isothiocyanate (FITC)-conjugated CD90 antibody. The representative images were presented from three independent experiments.

Figure 4. DMY regulated IL-1β induced FLSs proliferation and apoptosis. (A) FLSs were treated with a series of concentrations of DMY for 24 and 48 hours and results showed that there was no cytotoxicity of DMY. (B) Whereas, when exposed to DMY for 24 h and 48 h after the stimulation of 10 ng/mL IL-1β, FLSs in DMY-treated groups showed evident lower ability of proliferation than the vehicle. (C) FLSs were incubated with DMY (6.25, 12.5, 25 μM) for 24 h after the stimulation of 10 ng/mL IL-1β. Cell apoptosis was determined by Annexin V/PI staining. Populations in the upper-right quadrant of the flow cytometric graph represented apoptotic cells. (D) The percentage of apoptotic cells was quantified. All values represented mean ± S.E.M. of three independent experiments. $^{\#}P < 0.05$, $^{\#\#}P < 0.01$ versus the normal group; $^{*}P < 0.05$, $^{**}P < 0.01$ versus the vehicle-treated group.

Figure 5. DMY inhibits the migration of IL-1β induced FLSs. (A and C) Evaluation of the Boyden chamber experiment. FLSs were added to the upper chambers of transwells.

Representative images of three experiments were shown. Scale bar = 10 μm. (B) Cell migration was quantified by counting migrated cells in 9 microscope fields. The period of migration was determined at the time of 16 h. Values are the mean ± S.E.M. of at least 3 independent experiments. $^{**}P < 0.01$, $^{*}P < 0.05$ versus the group of 8 h. (E) The wound migration of FLSs derived from CIA rats. Representative photomicrographs of a scratch assay showed that the similar trend as the transwell-assay. Scale bar = 25 μm. (D and F) DMY dose-dependently attenuates cell migration. Values are the mean ± S.E.M. of at least three independent experiments. $^{\#}P < 0.05$, $^{\#\#}P < 0.01$ versus the normal group; $^{*}P < 0.05$, $^{**}P < 0.01$ versus the vehicle-treated group.

Figure 6. DMY regulates NF-κB signaling in FLSs. Cultured FLSs were stimulated with 10 ng/ml IL-1β. (A) DMY diminishes the production of inflammatory cytokines in FLSs, especially in higher doses. mRNA levels of cytokines were normalized to β-actin and the results were presented as fold decrease above IL-1β treatment (no DMY treatment). $^{*}P < 0.05$, $^{**}P < 0.01$ versus IL-1β stimulation. (B) The protein levels of phospho-IKK, -p65, and -IκB or total proteins were determined using Western blotting. With IL-1β stimulation (10 ng/ml) for indicated time to ensure that 15 min is the optimal time for the maximal activation of NF-κB signaling. $^{*}P < 0.05$, $^{**}P < 0.01$ compared with the untreated control. Thus, in co-incubation experiments (C), FLSs were treated with DMY for 24 h prior to stimulation with IL-1β for 15 min. $^{\#}P < 0.05$, $^{\#\#}P < 0.01$ compared with the IL-1β. (D) Effect of DMY on nuclear translocation of p65 in FLSs. Representative immunofluorescence photographs were showed as the staining of p65 localization is green and nuclei stained with DAPI is blue. (E) Molecular docking of IKKα and IKKβ with DMY. All values represent mean ± S.E.M. of three independent experiments.

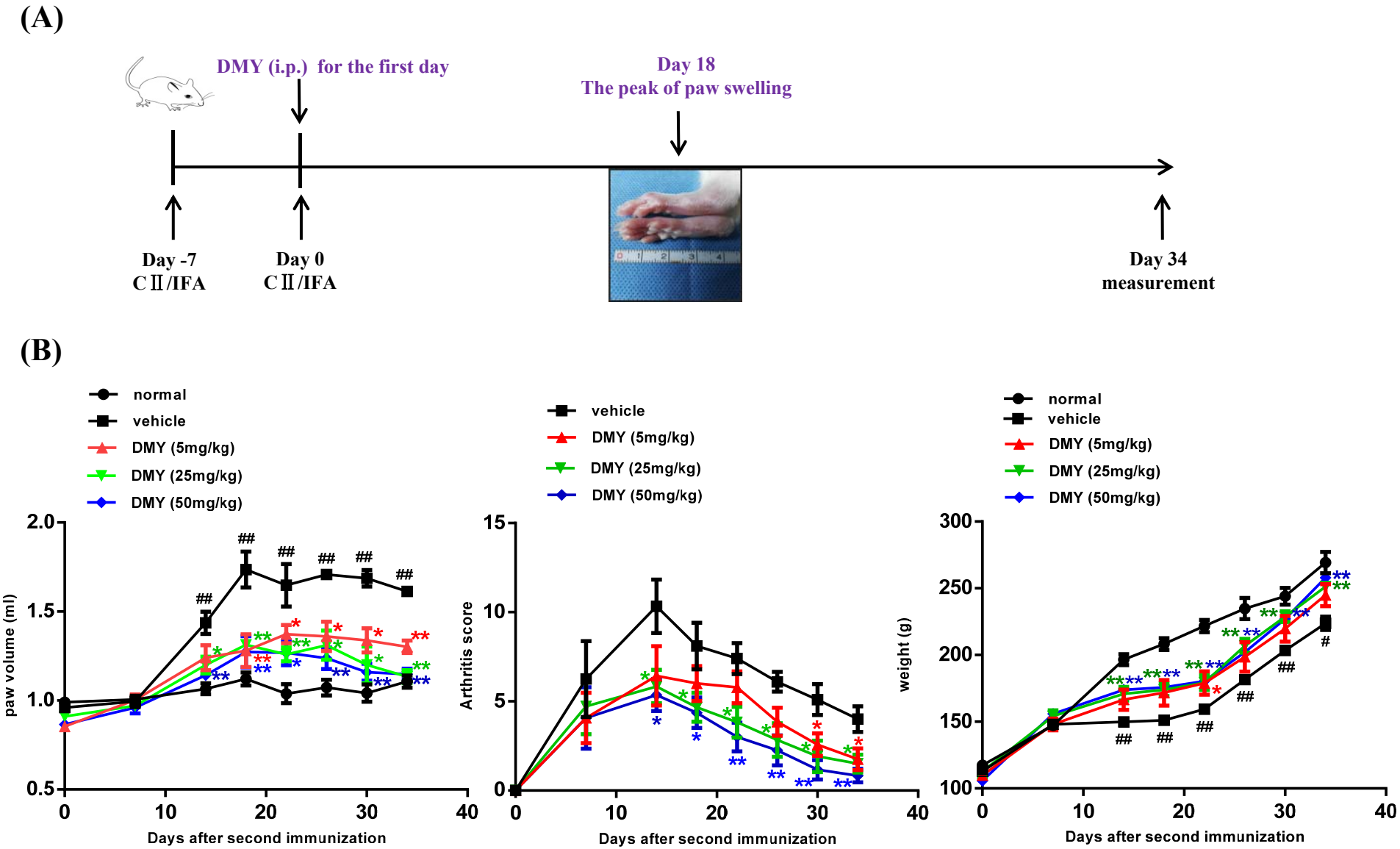

Fig. 1

(A)

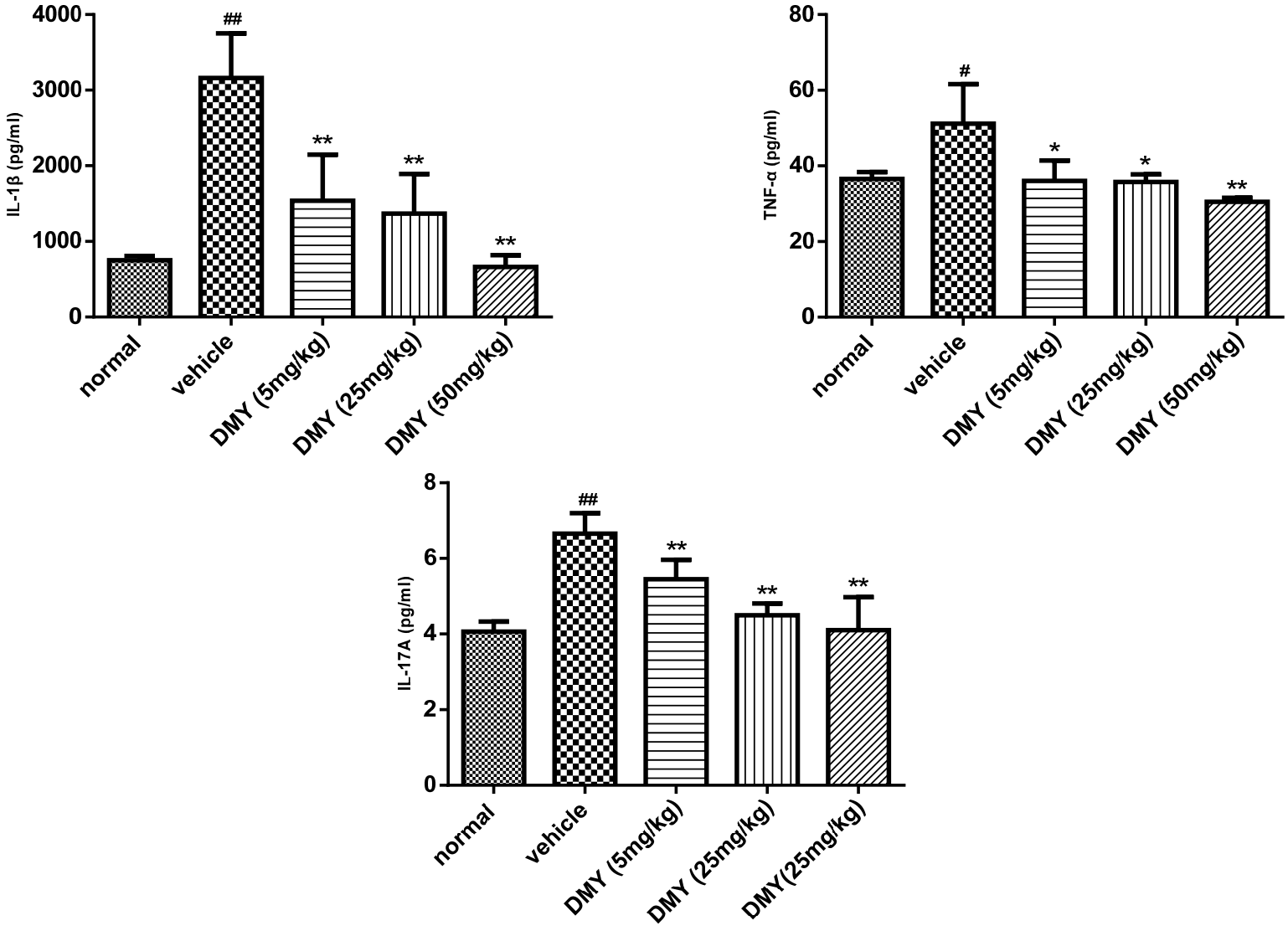

Fig. 2

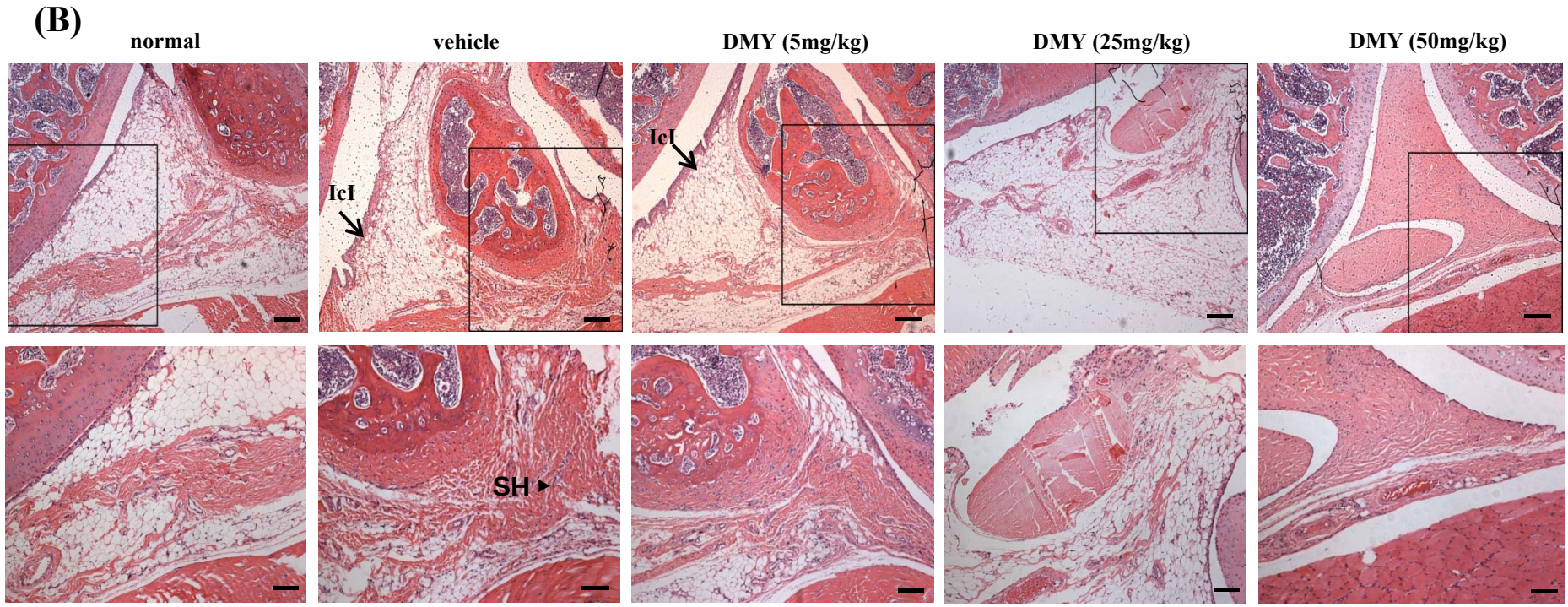

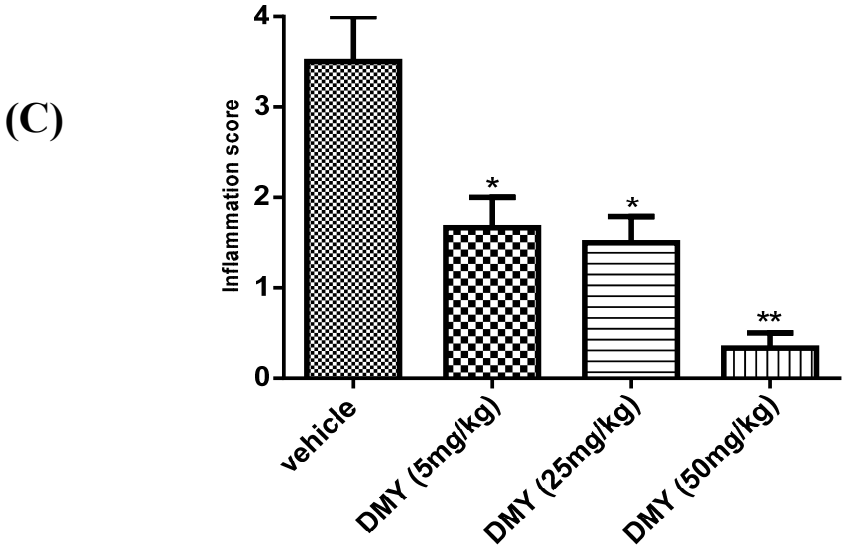

Fig. 2

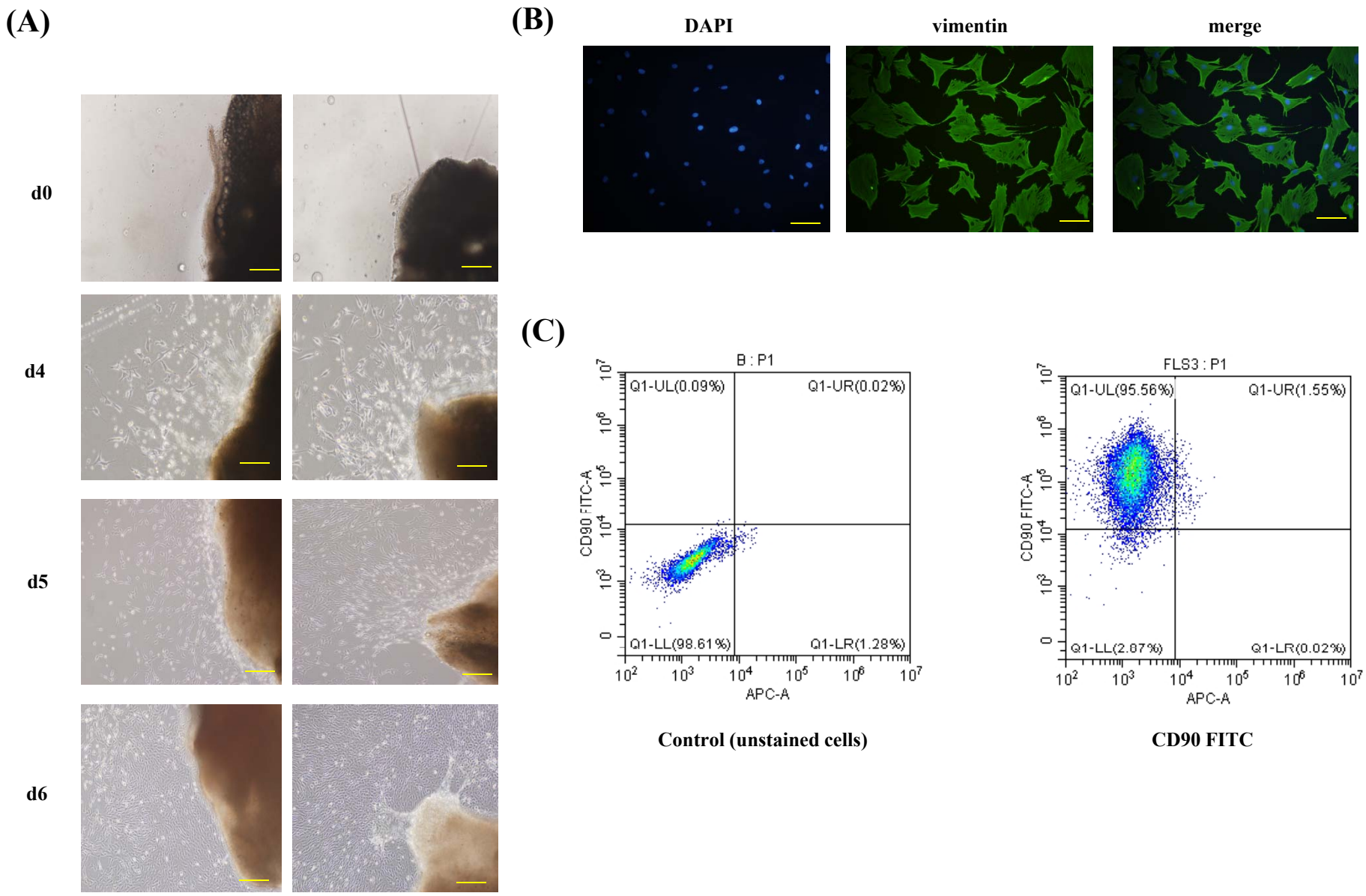

Fig. 3

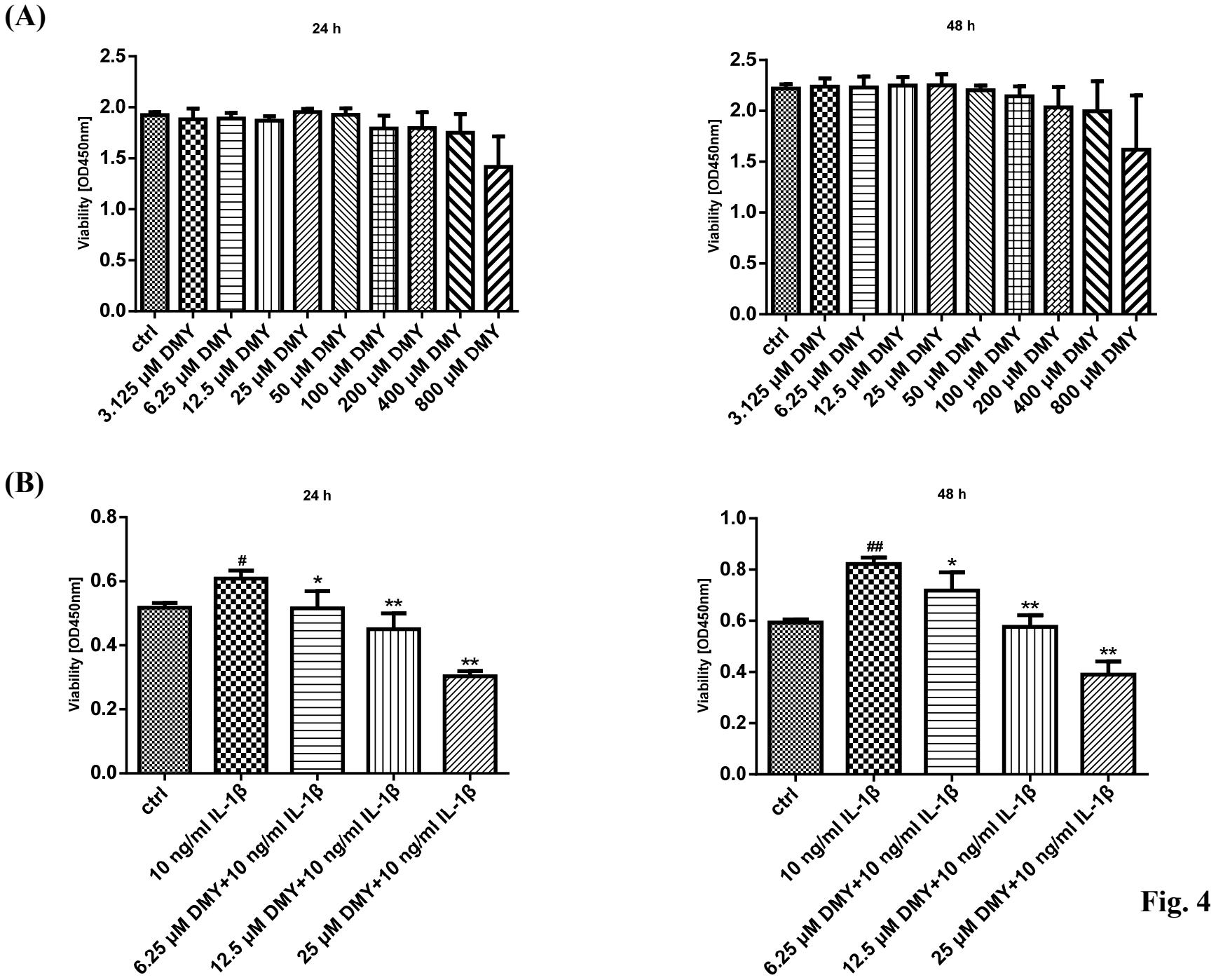

Fig. 4

(C)

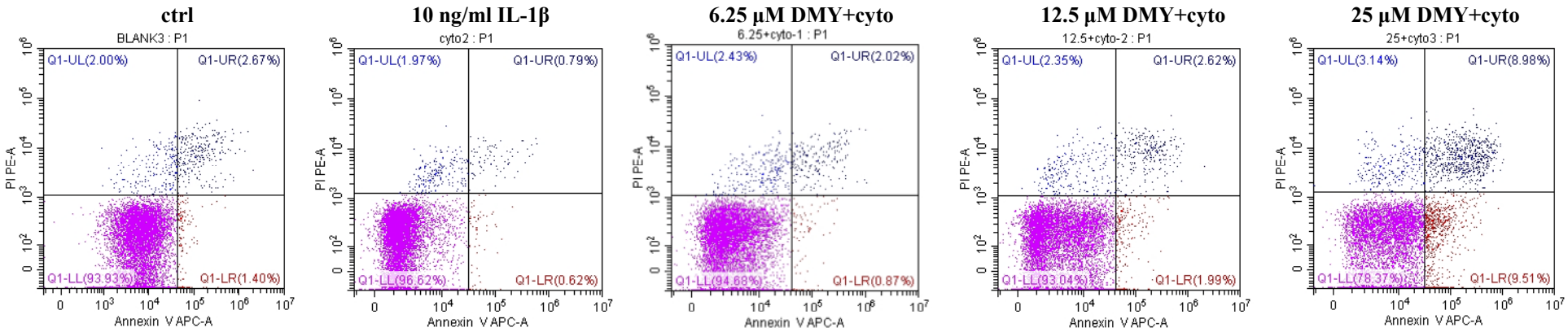

(D)

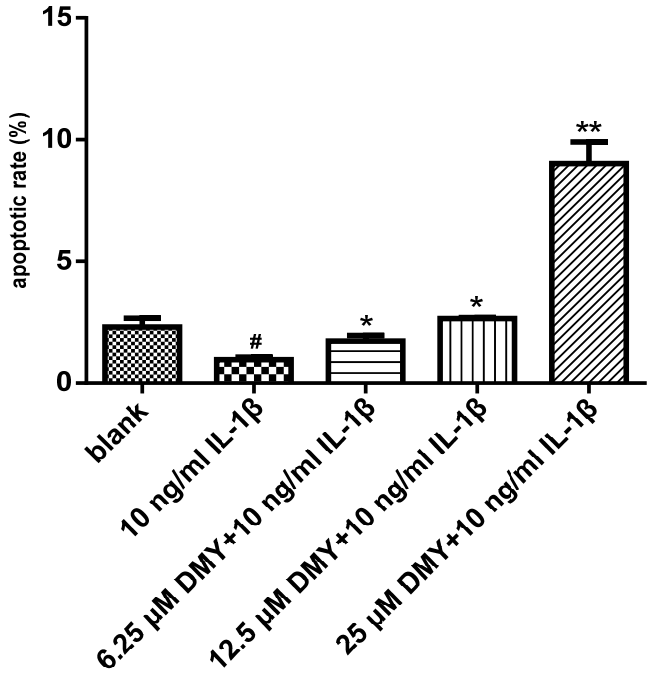

Fig. 4

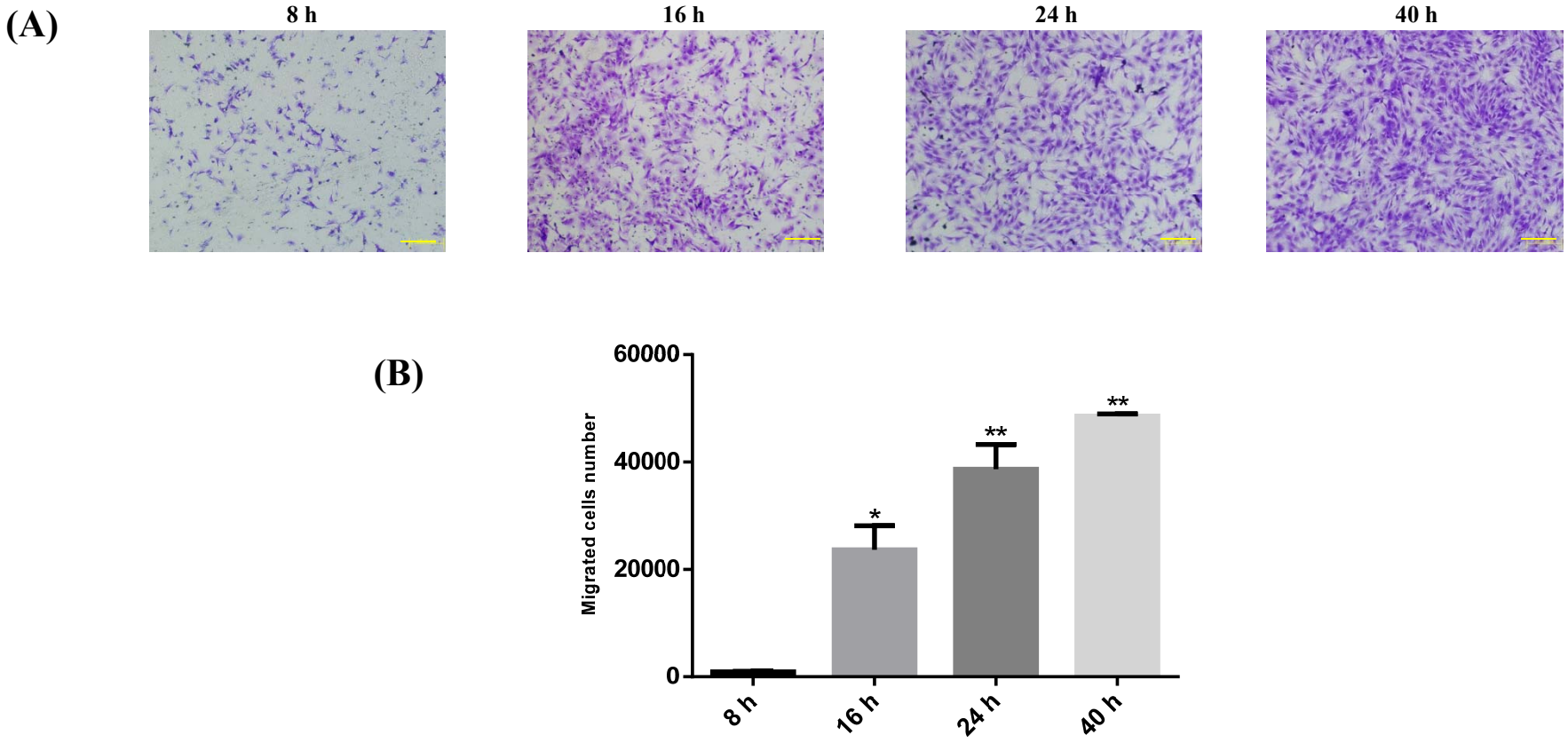

Fig. 5

(C)

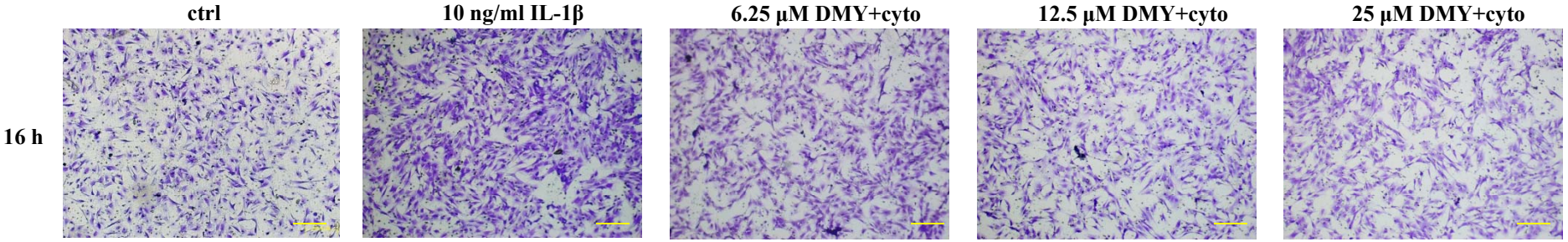

(D)

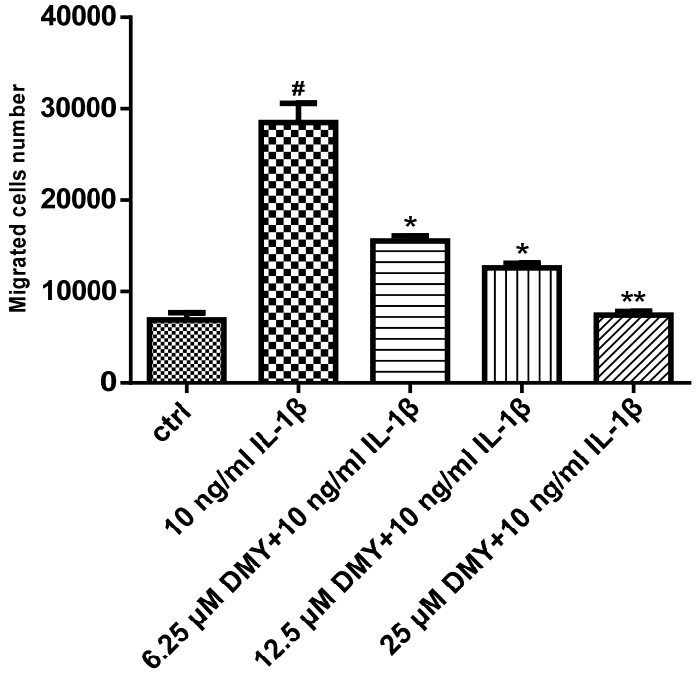

Fig. 5

Fig. 5

(F)

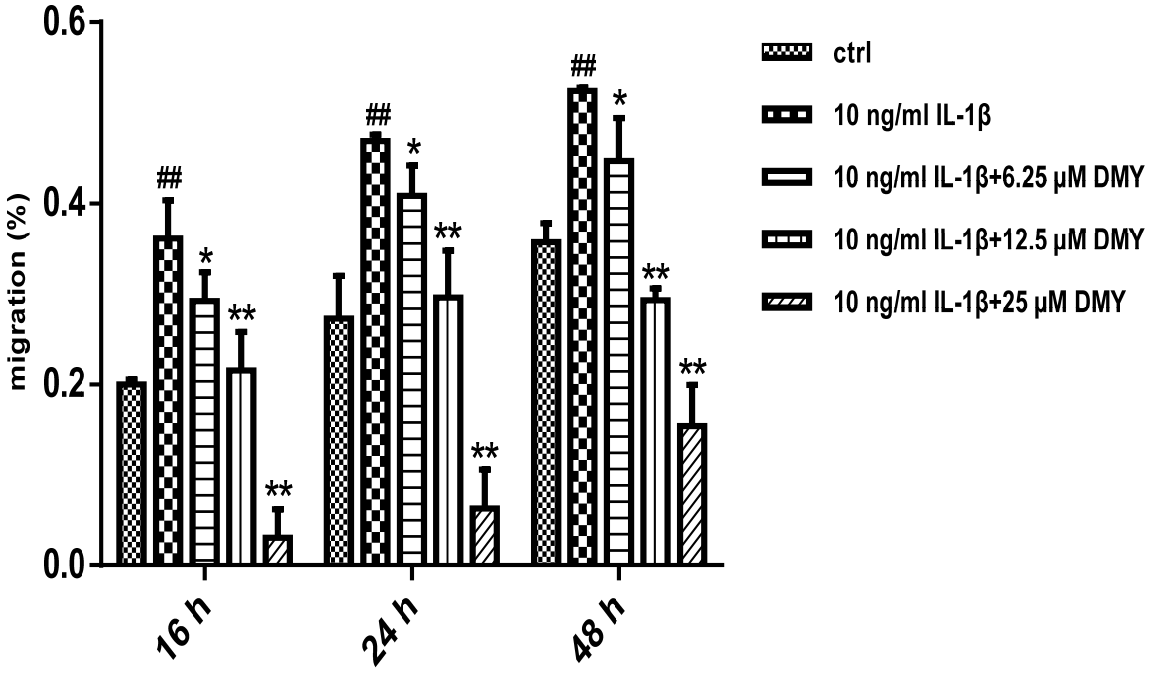

Fig. 5

(A)

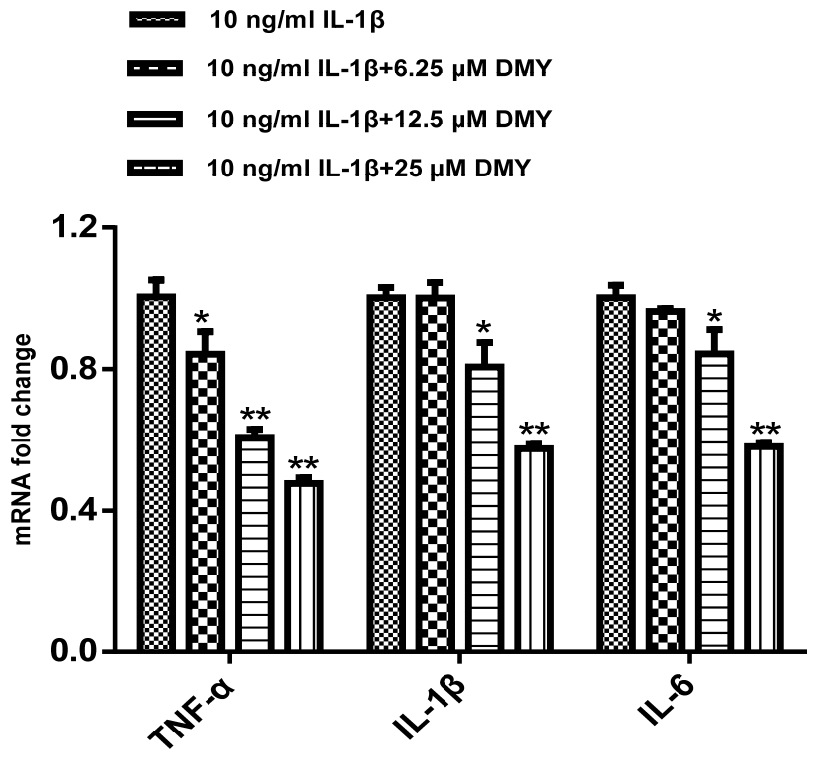

Fig. 6

(B)

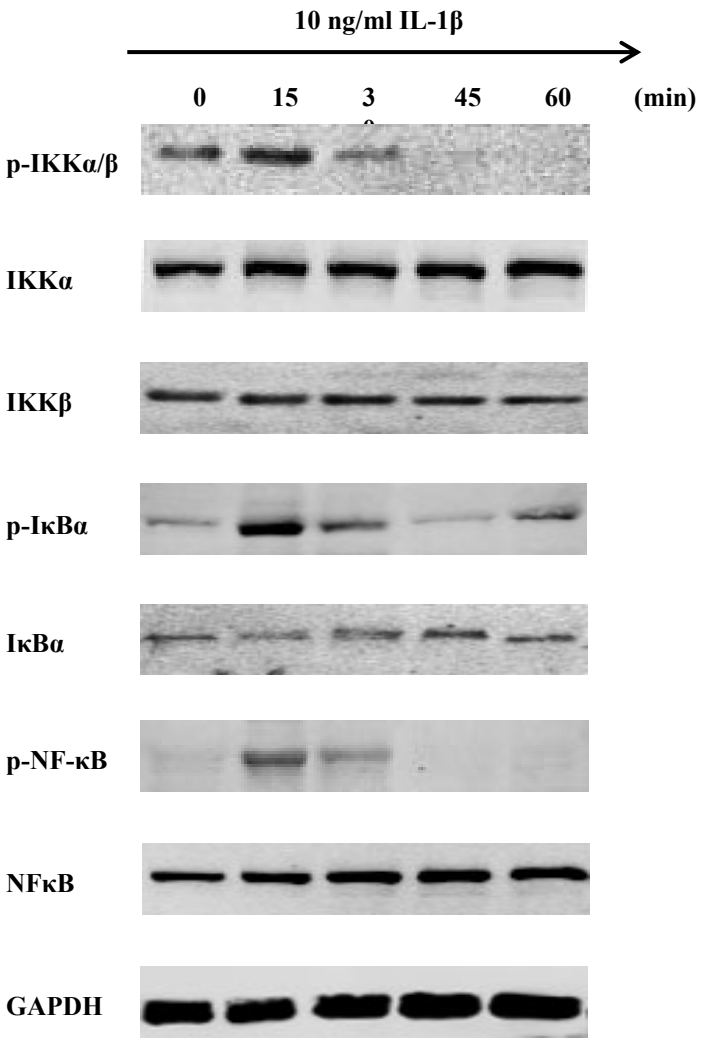

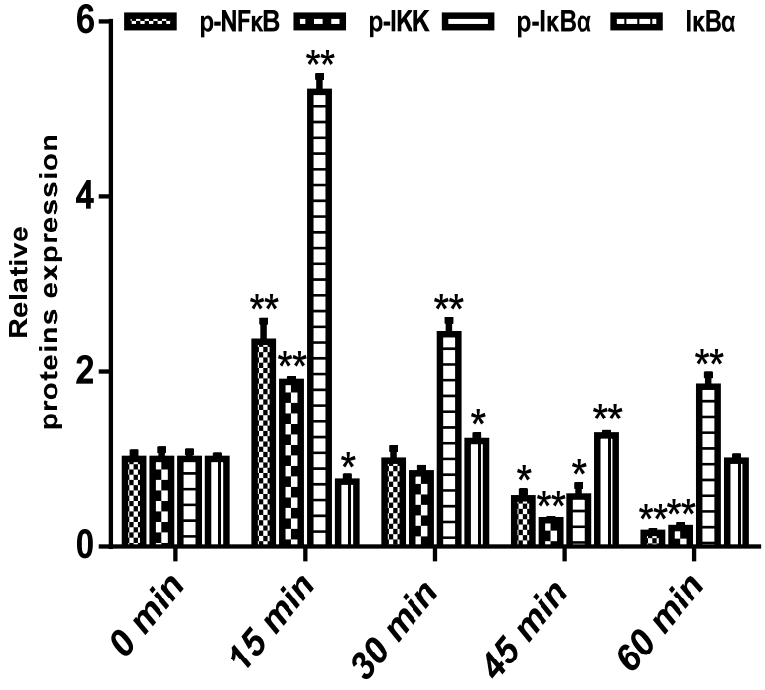

Fig. 6

(C)

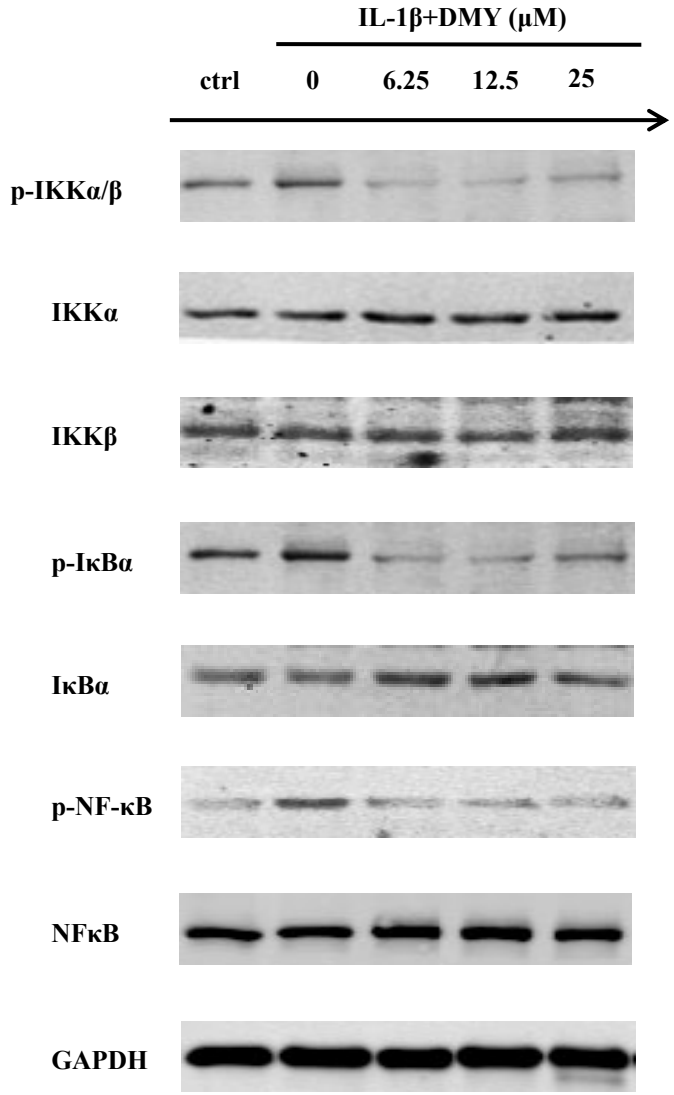

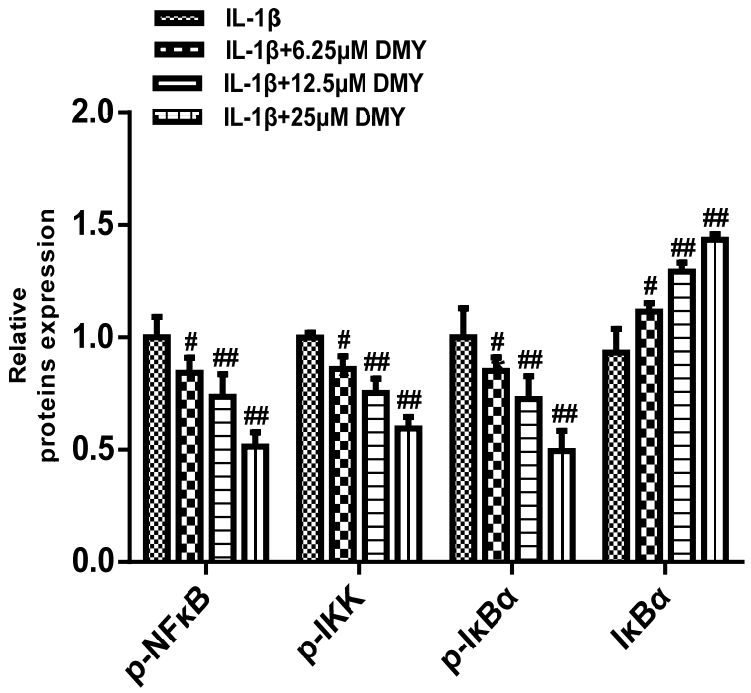

Fig. 6

Fig. 6

(E)

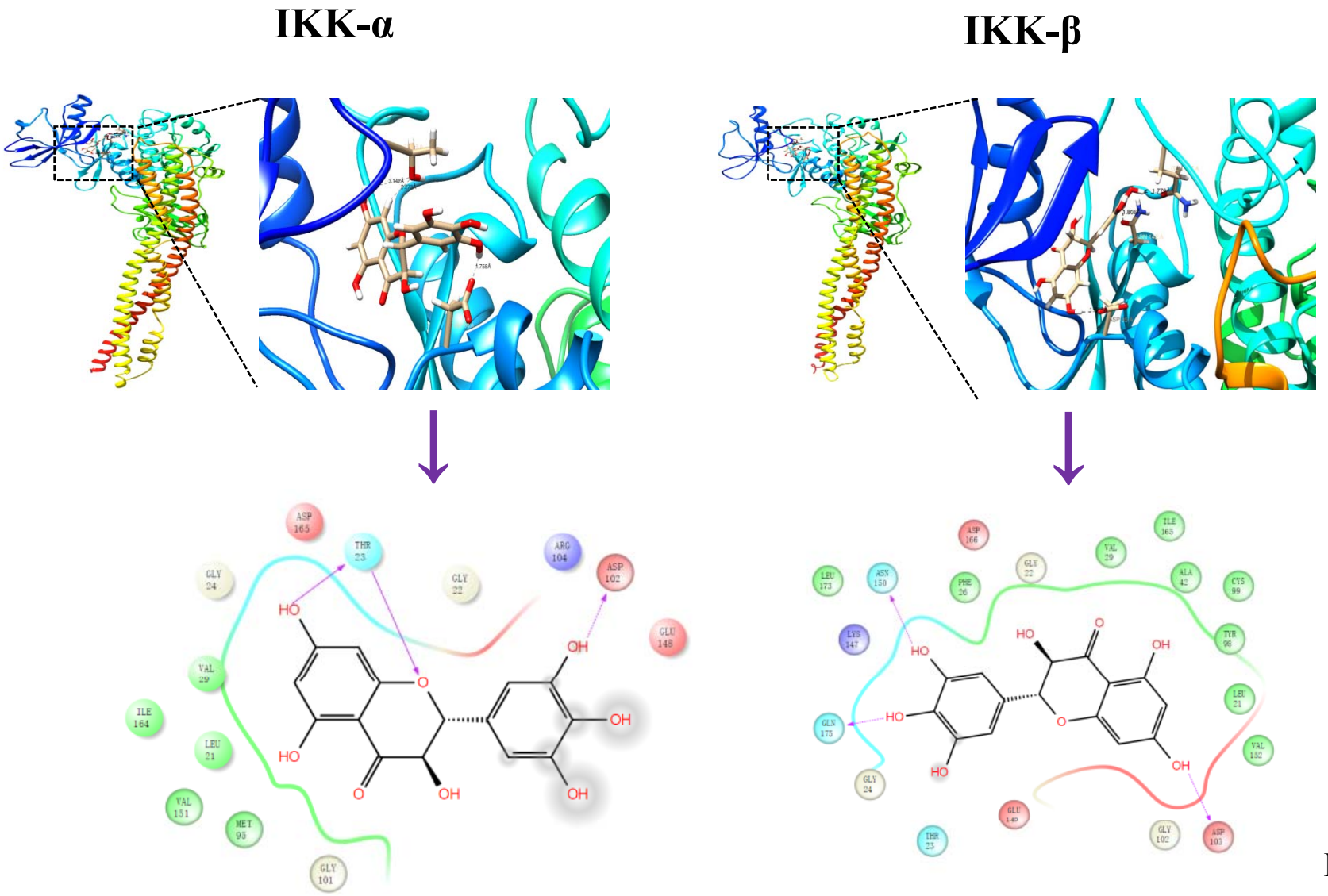

Fig. 6